CFD modeling of natural gas engine combustion with a flame area evolution model

Cite as: AIP Conference Proceedings **2191**, 020087 (2019); https://doi.org/10.1063/1.5138820
Published Online: 17 December 2019

G. Gianetti, L. Sforza, T. Lucchini, et al.

CFD Modeling of Natural Gas Engine Combustion with a Flame Area Evolution Model

G. Gianetti[1,a)], L. Sforza[1], T. Lucchini[1], G. D'Errico[1], P. Soltic[2], J. Rojewski[2] and G. Hardy[3]

[1]*Politecnico di Milano, Dip. di Energia, via Lambruschini 4, I-20156 Milan (Italy)*
[2]*Empa, Automotive Powertrain Technologies, Überland Str. 129, 8600 Dübendorf (Switzerland)*
[3]*FPT Industrial, Motorenforschung, Schlossgasse 2, 9320 Arbon (Switzerland)*

[a)]Corresponding author: giovannigaetano.gianetti@polimi.it

Abstract. A detailed description of the combustion process is fundamental in modern spark-ignition (SI) engines to guarantee control of pollutants formation and to meet future emission standards. Within this context, computational fluid dynamics (CFD) simulations represent an efficient and powerful tool to understand the different involved phenomena as mixture ignition, combustion development and pollutant formation. Object of this work is to find a CFD methodology to model premixed natural gas light-duty SI engines. The ignition stage is modeled by means of a simplified Eulerian spherical kernel approach (deposition model). Then, turbulent flame propagation is reproduced by means of two variables (regress variable and flame wrinkling factor) as proposed by Weller. Laminar to turbulent flame transition is taken into account using Herweg and Maly formulation and a zero-dimensional flame kernel radius evolution. Tabulated kinetics is used to estimate chemical composition of burned gases and to speed up the simulation since no chemical equilibrium calculations are necessary. The proposed CFD methodology was validated with experimental data of in-cylinder pressure, heat release rate and gross indicated work at different loads and speeds.

INTRODUCTION

The use of gaseous fuel, such as natural gas (NG), is one of the possible solution to reduce pollutant emissions, and in particular greenhouse gas from road transportation. The use of this fuel offers different advantages: first of all the low carbon content in natural gas leads to a reduction in CO_2 emission with respect to other fuel. Then, the use of a gaseous fuel limits the formation of particulate matter and the opportunity to use lean mixture reduces the emission of nitrogen oxides together with an increase of thermal efficiency. Moreover, it is possible to convert existing diesel compression ignition engines to natural gas spark-ignited by simply replacing the fuel injector with a spark plug and adding gas injectors in the intake manifolds. This approach reduces a lot the conversion costs and it is nowadays one of the most used and effective solution in the truck sector.

Within this context, a detailed description of all the processes that take place inside the combustion chamber becomes the only way to achieve low emissions and high efficiencies. To do that, reliable and detailed numerical models are essential for the development of efficient engines. Computational fluid dynamics (CFD) becomes a powerful tool to study combustion process since it allows to examine in detail all the associated phenomena, such as ignition, laminar to turbulent transition and fully turbulent combustion. The most used combustion model are the Coherent Flamelet Model (CFM) and G-Equation. The first one solves transport equations for the combustion progress variable c and the flame surface density field Σ, which is then used to compute the reaction rate [1]. The second is based on the level-set method and solves a transport equation for the non-reacting scalar G, avoiding the complications associated with counter-gradient diffusion and the need for a source term closure [2, 3]. Both models have been used for spark ignition engine simulations over the years [4]. On the other hand, it was demonstrated that CFM model fails in reproducing the qualitative behavior of flames near walls [5] and G-equation model presents a difficult implementation in CFD models, due to the different definitions of the G field and the constraints needed to avoid numerical instabilities and ensure geometrical consistency [6].

74th ATI National Congress
AIP Conf. Proc. 2191, 020087-1–020087-11; https://doi.org/10.1063/1.5138820
Published by AIP Publishing. 978-0-7354-1938-4/$30.00

This work presents a numerical methodology to model premixed combustion in light-duty, natural gas engines. The ignition process is described by means of a simplified Eulerian deposition model, while laminar to turbulent transition is handled by a semi-empirical model derived from [7]. A flame area evolution model was chosen for turbulent flame propagation, and in particular the one-equation model proposed by Weller is used. This model solves a transport equation for a combustion *regress* variable, b, while reaction rate depends on an algebraic expression of the flame wrinkling factor Ξ. The choice of a regress variable ensures numerical stability in the description of the flame propagation process and suitable expressions for Ξ can be directly taken from literature [3, 8]. Governing equations are modeled using RANS approach and standard $k - epsilon$ model is used for turbulence.

Validation of the proposed CFD methodology was performed on a natural gas light-duty SI engine at different loads and speeds. A comparison between numerical results and experimental measurements were performed in terms of in-cylinder pressure, heat release rate and gross indicated work.

NUMERICAL MODELS

The Weller or Flame Area Evolution model is based on the laminar flamelet assumption and is a one-equation model based on the laminar flamelet approach and it describes the flame development in the CFD domain by means of the flame wrinkling factor Ξ and the regress variable b. The first term, Ξ, is defined as the ratio between the turbulent and unstrained laminar flame speed S_t/S_u and it is formally related to the flame surface density Σ by:

$$\Sigma = \Xi \, |\nabla \tilde{b}| \tag{1}$$

The regress variable b represents the unburnt gas fraction in any computational cell, and its transport equation is derived by conditionally averaging the continuity equation on the unburned gas state [5, 9]:

$$\frac{\partial \rho \tilde{b}}{\partial t} + \nabla \cdot \left(\rho \tilde{\mathbf{U}} \tilde{b} \right) - \nabla \cdot \left(\mu_t \nabla \tilde{b} \right) = \rho_u \, \tilde{S}_u \, \tilde{\Xi} \, |\nabla \tilde{b}| + \dot{\omega}_{ign} \tag{2}$$

being μ_t the turbulent viscosity, S_u the unstrained laminar flame speed, ρ and ρ_u the mixture and unburned mixture density, respectively. The ignition source term is represented by $\dot{\omega}_{ign}$ while $\rho_u \tilde{S}_u \tilde{\Xi} |\nabla \tilde{b}|$ is the reaction rate due to turbulent flame propagation. Before the start of combustion, the regress variable field is uniformly equal to 1 in any computational cell. Equation 2 can be solved fully implicitly by exploiting differential operator properties. This ensures a stable solution for the flame propagation process even in presence of complex meshes and long time-steps.

Ignition model

The main purpose of the ignition model is to provide an initial distribution for the regress variable to start the flame propagation process. A simplified deposition model was used in this work [10], while more complex approaches already validated by the authors will be integrated in the proposed approach in future works [11, 12, 13]. The user specifies an initial flame kernel diameter d_{ign} and time interval Δt_{ign}; in the cells whose distance from the spark plug is less than $r_{ign} = d_{ign}/2$ an ignition source term is imposed:

$$\dot{\omega}_{ign} = \frac{C_s \, \rho_u \, b}{\Delta t_{ign}} \tag{3}$$

where C_s is a user-defined strength parameter, Δt_{ign} is the user-specified ignition duration and ρ_u is the unburned gas density. The deposition model is suitable for simplified spark-ignition combustion simulations in engines, because:

- the source term $\dot{\omega}_{ign}$ can be user-calibrated without significant effects on the heat release rate profile,
- the regress variable b is gradually initialized, going smoothly to zero only in a small volume around the spark-plug.

Moreover, due to the implicit formulation, it does not produce any unphysical effect in those cells where the b value is already zero.

Turbulent combustion model

The regress variable distribution produced by the ignition model is suitable for the propagation of a premixed flame. However, according to first RHS term of Eqn. 2, it is necessary to find a proper expression for the flame wrinkling factor Ξ that allows the flame front evolution from its initial laminar features to a fully developed turbulent flame.

According to one-equation Weller model [5], the Ξ distribution has a twofold dependency: the first on its equilibrium value $\Xi^* = f(\Xi^*_{eq})$, the second on the regress variable b as shown by the following expression:

$$\Xi = 1 + [1 + 2\, S_\Xi\ (0.5 - b)]\ (\Xi^* - 1) \tag{4}$$

Here, the dependency on Ξ^*_{eq} is due to the fact that laminar to turbulent flame transition is completed when Ξ reaches the value resulting from the equilibrium between production and merging (destruction) of reaction layer corrugations. This last condition is called *equilibrium* and it is characterized by the maximum wrinkling factor value, corresponding to Ξ^*_{eq}. On the other hand, the dependency of Eqn. 4 on b mimics the turbulence distribution across the flame, which is calibrated through the user defined constant S_Ξ. However, as a starting point, only Eqn. 4 dependency on Ξ^* was considered, leaving to further studies the analysis on b influence; therefore, S_Ξ was set to zero in this work.

The presence of $\Xi^* = f(\Xi^*_{eq})$ in Eqn. 4, instead of directly Ξ^*_{eq}, is necessary to properly consider a *transition* between laminar and turbulent regimes. In fact, its value is expressed as follows:

$$\Xi^* = S_t / S_u = I_0 + I_0^{1/2}\ f\ \left(\Xi^*_{eq} - 1\right) \tag{5}$$

where I_0 is the flame stretch coefficient, while parameter $0 \leq f \leq 1$ is used to model the flame evolution from laminar ($f = 0$) to turbulent ($f \to 1$) features. Following Herweg and Maly approach [14], f is computed as:

$$f = \left[1 - exp\left(-\frac{r_k}{\langle L_t \rangle}\right)\right]^{0.5} \left[1 - exp\left(-\frac{\langle u' \rangle + \langle S_u \rangle}{\langle L_t \rangle}\ t_{ign}\right)\right]^{0.5} \tag{6}$$

where t_{ign} is the time elapsed from spark timing, r_k is the flame kernel radius estimated by a 0-D model, while L_t and u' are the turbulence intensity and integral length scale, respectively. The expression $\langle \cdot \rangle$ denotes an operation of field averaging on a spherical volume with radius of $C_{vol} r_k$ around the spark-plug, being C_{vol} a user-defined constant.

For what concerns the 0-D model for Eqn. 6 kernel radius estimation, initially the flame is assumed to be laminar and r_k is computed from:

$$\frac{dr_k}{dt} = \frac{\rho_u}{\rho_b}\ I_{0,lam}\ S_u \tag{7}$$

being ρ_b the burnt mixture density and $I_{0,lam}$ is the laminar flame stretch parameter. This last value can be computed according to:

$$I_{0,lam} = \left(1.0 - \frac{\mathcal{L}_u \kappa}{S_u}\right) \tag{8}$$

where $\mathcal{L}_u$ is the Markstein length referred to unburned gases while κ is the flame strain rate

$$\kappa = \frac{2}{r}\frac{dr}{dt} \tag{9}$$

assumed spherical the kernel geometry. Then, when kernel size exceeds a threshold value $r_{k,trans}$, which is defined as a multiple of the Taylor turbulence micro-scale λ [15]:

$$r_{k,trans} = C_{Tay}\ \lambda = C_{Tay}\ \sqrt{10\ \nu\ \frac{k}{\varepsilon}} \tag{10}$$

being C_{Tay} the multiplicative coefficient, dr_k/dt is computed according to Herweg and Maly expression for turbulent flames [14]:

$$\frac{dr_k}{dt} = \frac{\langle \rho_u \rangle}{\langle \rho_b \rangle}\ \left[I_0 + I_0^{1/2} f' \left(\left\langle \Xi^*_{eq} \right\rangle - 1\right)\right]\ \langle S_u \rangle \tag{11}$$

Concerning the modeling of laminar to turbulent flame transition, Eqn. 6 was slightly modified as follows

$$f' = \left[1 - exp\left(-\frac{r_k - C_{Tay}\,\lambda}{\langle L_t \rangle}\right)\right]^{0.5} \left[1 - exp\left(-\frac{\langle u' \rangle + \langle S_u \rangle}{\langle L_t \rangle}\, t_{ign}\right)\right]^{0.5} \tag{12}$$

in order to compute coefficient f' with respect to the kernel dimension relative to Taylor micro-scale. This solution was adopted to make the 0-D model and Eqn. 10 more consistent. During flame kernel growth, to ensure continuity in Eqn. 11 between the dr_k/dt expression and both turbulence and laminar stretch effects, the I_0 coefficient is computed as:

$$I_0 = min\left(I_{0,lam}, I_{0,turb}\right) \tag{13}$$

where the empirical relation from Bray [16] is used to estimate $I_{0,turb}$:

$$I_{0,turb} = \frac{0.117}{1+\tau} Ka^{-0.784} \tag{14}$$

in which Ka is the Karlovitz number and $\tau = T_b/T_u - 1$.

Equilibrium wrinkling factor correlation

The expression for Ξ^*_{eq}, necessary for computing Eqns. 5 and 11, is taken from Gulder [17]:

$$\Xi^*_{eq} = 1 + \Xi_{coef} \sqrt{\frac{u'}{S_u}} \mathcal{R}_\eta \tag{15}$$

where Ξ_{coef} is equal to 0.62, value obtained with an interpolation of many sets of experimental data in [17]. $\mathcal{R}_\eta$ is the Kolmogorov Reynolds number, defined as:

$$\mathcal{R}_\eta = u' / \left(\varepsilon\, \tau_\eta\right) \tag{16}$$

$$\tau_\eta = \sqrt{\mu_u / \left(\rho_u\, \varepsilon\right)} \tag{17}$$

Here, ε is the turbulence kinetic energy dissipation rate, τ_η the Kolmogorov time scale and μ_u the dynamic viscosity of unburned mixture.

Laminar flame speed correlation

Unstrained laminar flame speed S_u is estimated according to:

$$S_u = S_{u,ref}\left(\phi\right) \cdot \left(\frac{T}{T_{ref}}\right)^{\alpha} \cdot \left(\frac{p}{p_{ref}}\right)^{\beta} \tag{18}$$

where $S_{u,ref}$ depends on equivalence ratio and is computed at reference conditions. Because Natural Gas was assumed to be Methane, the laminar flame speed $S_{u,ref}$ value was computed according to [18]:

$$S_{u,ref} = W \cdot \phi^{\eta} \cdot e^{-\xi(\phi - 1.075)^2} \tag{19}$$

Coefficients W, η, ξ, α, β are available in [18] for propane, methane and iso-octane fuels and they are validated up to 20 bar and 450 K. For higher values, which are typically reached inside an internal combustion engine, it has to be taken into consideration an error of approximately 30% on the laminar flame speed. The only way to improve the estimation of S_u seems to be the use of a detailed kinetic mechanism to compute and tabulate laminar flame speed values, since correlations present a limited range of validity.

Tabulated Kinetics

The chemical composition in any computational cell is obtained from regress variable b, mass fraction of chemical species in the burned $Y_{b,i}$ and unburned $Y_{u,i}$ state as:

$$Y_i = b \cdot Y_{u,i} + (1 - b) \cdot Y_{b,i} \tag{20}$$

Burned gas chemical composition $Y_{b,i}$ is computed from a lookup table and the methodology is accurately described in [19]. Reaction rates and chemical composition are stored in a lookup table, which is generated by processing results of constant-pressure homogeneous reactor calculations. These computations were performed at different values of equivalence ratio (from 0 to 1 using a step of 0.1), pressure (from 1 bar to 20 bar using a step of 5 bar and from 20 bar to 120 bar using a step of 10 bar) and unburned gas temperature (from 400 K to 1000 K using a step of 50 K), using the GRI 3.0 mechanism with 53 species and 325 reactions. In this work, only chemical composition at equilibrium conditions is retrieved while reaction rate from premixed combustion comes from Eqn. 2. In a future work, homogeneous reactor reaction rates can be used in combination with Weller model to successfully predict dual-fuel or spark-assisted combustion.

To correctly access to the lookup table, a transport equation is solved for the unburned gas enthalpy h_u, which provides the fresh charge temperature T_u. Burned gas enthalpy h_b is estimated from h_u and the mean cell value:

$$h_b = \frac{h - b \cdot h_u}{1 - b} \tag{21}$$

Accordingly, the burned gas temperature T_b is computed from h_b and composition Y_i, b.

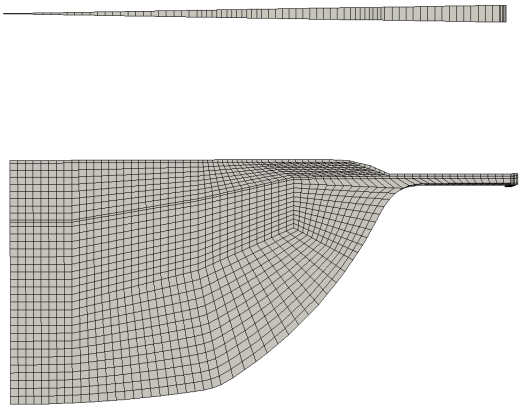

FIGURE 1. Computational mesh of the light-duty engine.

EXPERIMENTAL VALIDATION

Validation of the presented models was carried out on the experimental data of light duty SI engine fueled with natural gas at different operating conditions. Main engine data are reported in Tab. 1.

The computational grid used in this work and reported in Fig. 1 is a 2D representation of half of the combustion chamber. It was generated using a block structured grid in order to control cell dimension and shape. Mean cell length is around 0.7 mm and mesh size goes from 5000 cells at Top Dead Center (TDC) up to a maximum of 10600 cells at Inlet Valve Closing (IVC). The grid was moved using the dynamic mesh layering technique presented in [20].

In order to test a wide range of the engine map, thirteen different operating points were simulated. Tab. 2 reports main engine parameters of the simulated points. Starting from the condition named D65, it was decided to vary the engine speed from 1400 rpm to 3000 rpm with a step of 200 rpm, and the engine load from 30% to 80%.

Numerical simulations were run using the open-source software OpenFOAM® coupled with the LibICE code, a set of libraries and solver for internal combustion engines. Governing equations were modeled using RANS approach

TABLE 1. Main geometry data of the light-duty SI engine.

Displaced volume	3.0 L
Stroke	104 mm
Bore	95.8 mm
Connecting rod	160 mm
Compression ratio	12.5:1
Number of valves	4

TABLE 2. Simulated operating points of the gas natural light duty engine.

Number	Name	Speed [rpm]	Load [%]
1	A50	1400	50
2	B50	1600	50
3	C50	1800	50
4	D30	2000	30
5	D40	2000	40
6	D50	2000	50
7	D65	2000	65
8	D80	2000	80
9	E50	2200	50
10	F50	2400	50
11	G50	2600	50
12	H50	2800	50
13	I50	3000	50

and standard $k-\varepsilon$ model was used for turbulence. EGR was not used for these operating conditions and for this reason only one chemistry table was generated. Heat transfer was predicted using Angelberger model [21]. Simulations were run from inlet valve closing to Exhaust Valve Opening (EVO) on 8 cores and each operational point was completed in 1 hour approximately for the 2D case and 24 hours for the 3D (Intel Xeon E5-2637 v2 @3.50 GHz). Thermodynamic conditions at IVC were derived from GT-Power data, whereas flow motion and turbulence inside the cylinder were initialized knowing piston speed and swirl number, as explained in [22]. Model constants used for ignition and turbulent combustion are reported in Tab. 3.

Ignition and turbulent combustion tuning

The medium load point D65 running at 2000 rpm was used to tune the ignition and turbulent combustion constants. Figure 2 reports in-cylinder pressure and Apparent Heat Release Rate (AHRR) values of this operational point. Computed data are compared with experimental ones and normalized by their maximum value. Calculated and experimental pressure curves are overlapped for most of the time except for the pressure peak, which is slightly overestimated by the CFD simulation. Computed AHRR curve is in good agreement with the experimental one during the ignition, laminar to turbulent and fully turbulent combustion phases. Towards the end of combustion instead, in the range of 10-30 CAD, the heat release rate slows down in both computed and experimental data. This behavior, noticed also by

TABLE 3. Model constants used for ignition and turbulent combustion.

Initial flame kernel d_k	4 mm
C_{vol}	10.0
Ratio $C_s/\Delta t_{ign}$	2/3
Ξ_{coef}	0.6

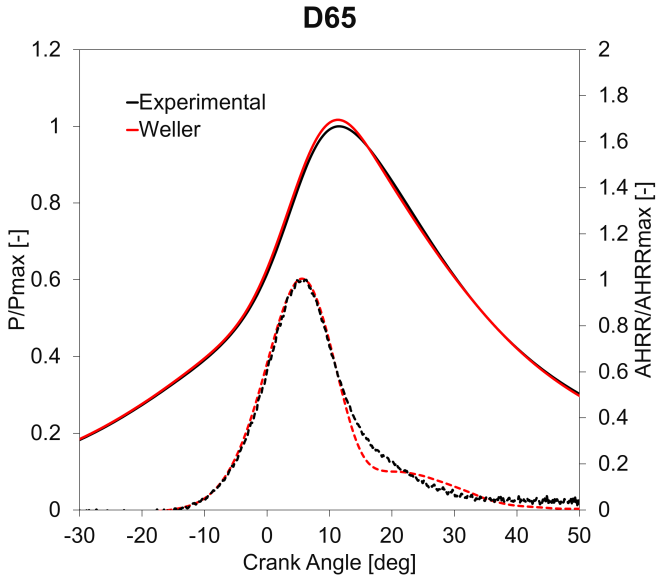

FIGURE 2. Comparison between experimental and computed data of in-cylinder pressure (*solid* lines) and apparent heat release rate (*dashed* lines) of operating point D65.

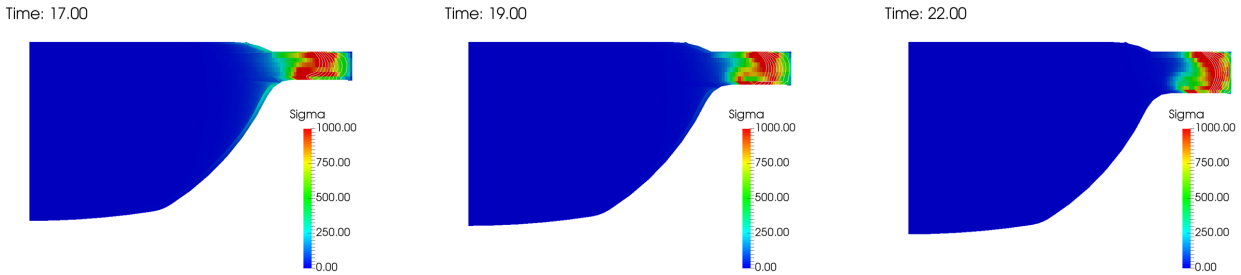

FIGURE 3. Flame surface density distribution and contour plot of regress variable at 17, 19 and 22 degrees after TDC for operating point D65.

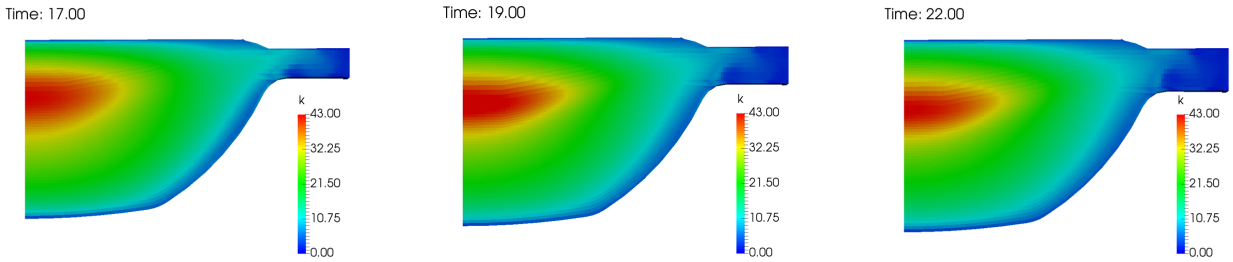

FIGURE 4. Turbulent kinetic energy distribution at 17, 19 and 22 degrees after TDC for operating point D65.

Reyes et al. in [23], could be due to the diesel bowl geometry, which is not optimized for spark ignition combustion. Looking at the flame evolution reported in Fig. 3, it is possible to notice that the slow slope of heat release rate mentioned before occurs when flame reaches the squish band. Inside this region, the turbulence is definitely lower with respect to the bowl, as shown in Fig. 4. This aspect leads to a slower combustion of a quite large fuel fraction in a less-favorable flame propagation environment. However, looking always at Fig. 2, computed AHRR present a plateau

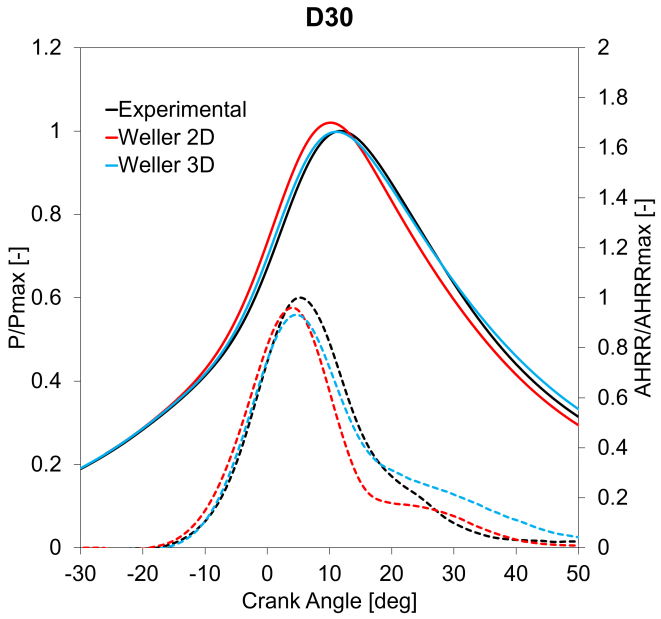

FIGURE 5. Comparison between experimental and computed data (2D and 3D) of in-cylinder pressure (*solid* lines) and apparent heat release rate (*dashed* lines) of operating point D30.

around 20 CAD which is absent in the experimental curve. A possible explanation for this behavior could be the use of a 2D geometry with a turbulence field that is imposed at IVC. These simplifications are reasonable for testing the predictive capabilities of the combustion solver in a wide range of operating conditions with a limited computational effort. On the other hand, a full 3D geometry initialized with the correct flow field can certainly give a more detailed description of the turbulence distribution inside the combustion chamber, with an improvement on the heat released during late combustion, but it requires an important increase of computational time.

Full 3D geometry simulation

In order to study the main differences between 2D and 3D, low load point D30 running at 2000 rpm was simulated considering also the full geometry. In Fig. 5 are reported the experimental and computed in-cylinder pressures and apparent heat release rates. The overall trend of pressure curves is rather similar for 2D and 3D case, even if it is possible to notice a small anticipation and overestimation a of the pressure peak by the 2D case with respect to the 3D and the experimental data. This aspect becomes more clear looking at the AHRR curves: the 2D case shows a faster laminar to turbulent transition with respect to 3D and this leads to the anticipation and overestimation of the pressure peak. To better understand this aspect Fig. 6 compares the turbulence distribution and the regress variable contour plot near the spark plug at -20 CAD for the two cases. The presence of the spark plug in the 3D case modifies a lot the turbulence in this region, slowing down the flame kernel growth and the laminar-turbulent transition.

Another important difference that can be noticed always in Fig. 5 is the heat released during late combustion: as mentioned before, both simulated AHRR curves show a slow slope around 20 CAD. In the 2D case this behavior is more evident than in the 3D one, and it is probably due to the non-axisymmetry of the combustion chamber. Looking at Fig. 7, which reports the regress variable distribution inside the combustion chamber at 20 CAD, it is possible to notice that the flame has reached the squish region in the right part of the 3D case, exactly as the 2D case. On the other hand, on the left part of the full geometry case, which is characterized by a flat cylinder head, the flame has not reached completely the squish region. These non-homogeneous flame distribution leads to a different AHRR curves, with the 3D case that is more similar to the experimental one with respect to the 2D.

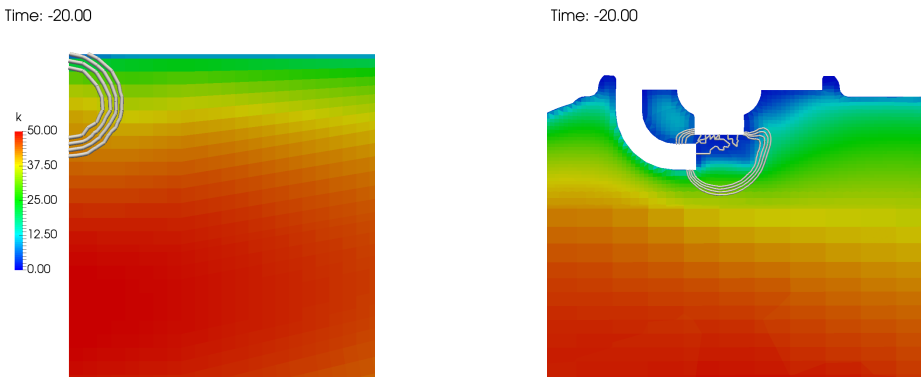

FIGURE 6. Turbulence distribution and regress variable contour plot inside the combustion chamber for 2D (left) and 3D (right) cases at -20 CAD.

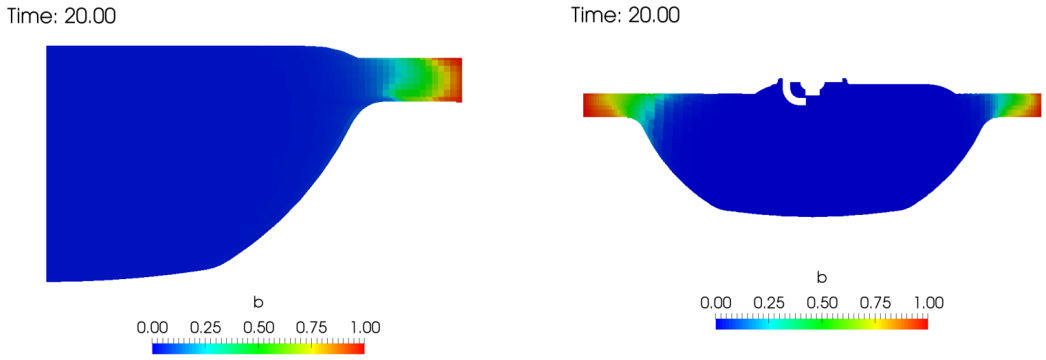

FIGURE 7. Regress variable distribution inside the combustion chamber at 20 CAD for the 2D (left) and 3D (right) cases.

Validation on other operating points

After the calibration of the model constants the flame area evolution model was tested on all the other twelve operating points. Figure 8 provides an overview on the model capabilities to predict the in-cylinder maximum pressure and the work produced by the engine at these conditions. More specifically, the graph on the left of Fig. 8 reports on the x-axis the experimental maximum cylinder pressure and on the y-axis the computed ones, all normalized by the measured maximum pressure. In case of a perfect matching between computed and experimental data, all points would lie on the dotted black line which represents the quadrant bisector. Computed maximum pressures are in rather good agreement with experimental ones, except for one point, the low load conditions D40. The error percentage of this operating point is around 10% and it is probably due to an incorrect composition of the gases at IVC: all the simulations start with the same gas composition, considering a certain quantity of gas trapped from the previous cycle. It is reasonable to assume that residual gases are higher at low loads with respect to medium-high points. An underestimation of the residual gases results in an overestimation of the oxygen mass fraction in the combustion chamber that leads to higher pressure peaks.

Finally, looking at the graph on the right of Fig. 8, which compares experimental and computed normalized gross indicated work, it is possible to notice that most of points lie close to the quadrant bisector. The percentage error is below 3% for all the analyzed conditions except for the medium-high load point D80 which has an error around 5%.

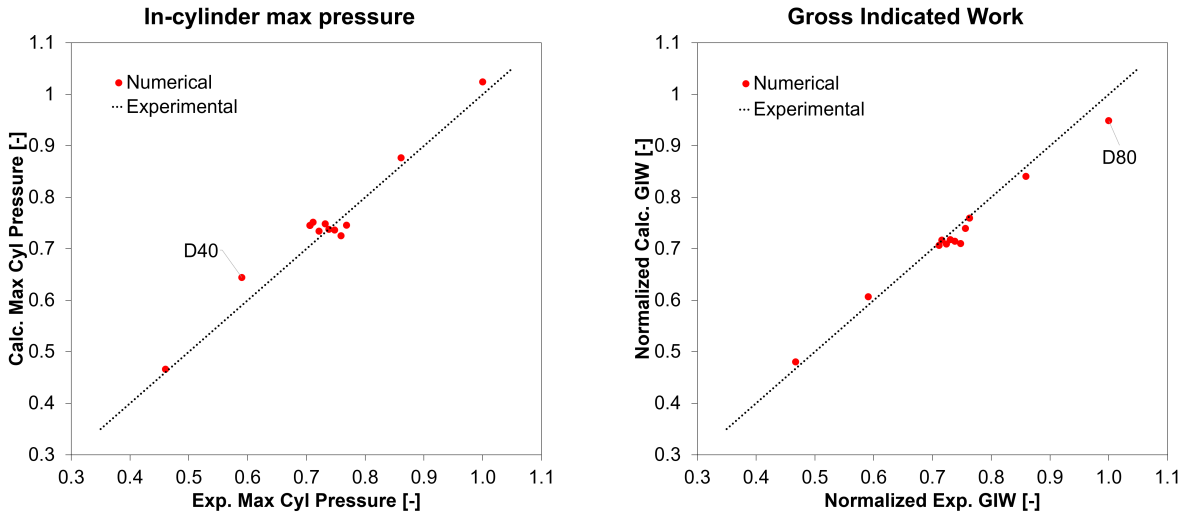

FIGURE 8. Experimental and computed maximum cylinder pressure (left) and gross indicated work (right) for all the thirteen operating points.

CONCLUSION AND FUTURE DEVELOPMENT

The main scope of this work was to find a CFD methodology for the combustion modeling of natural gas SI light-duty engines. A simplified Eulerian spherical kernel approach was used to model the ignition process whereas a flame area evolution model for the turbulent flame propagation. The one-equation model proposed by Weller was chosen due to the limited number of tuning constants and to ensure numerical stability. The proposed methodology was validated using experimental data of a light-duty engine, tested at different loads and speeds.

Results in terms of pressure, heat release rate and gross indicated work show that the methodology can be applied with rather satisfactory results. Low load point D40 probably needs a more detailed description of boundary conditions to improve results. Moreover, simulation of a full 3D geometry seems to be the best solution to obtain a more precise description of the phenomena, in particular when the flame reaches the squish region.

Future works on the proposed model are the analysis of the regress variable influence of Ξ, which mimics the turbulence distribution across the flame and the tabulation of the laminar flame speed and thickness using a reaction mechanism. In the meantime, the combustion solver will be tested considering also the presence of EGR and using the whole 3D geometry to overcome the limitation described in this work.

REFERENCES

[1] F. E. Marble and J. E. Broadwell, "The Coherent Flame Model for turbulent chemical reactions," Tech. Rep. (TRW Defense and Space Systems Group, 1977).

[2] M. Herrmann, "Refined Level Set Grid method for tracking interfaces," (2005).

[3] N. Peters, *Turbulent Combustion* (Cambridge University Press, 2000).

[4] A. d'Adamo, S. Breda, S. Fontanesi, and G. Cantore, SAE Int. J. Engines (2015).

[5] H. G. Weller, Thermo-Fluids Section Report TF 9307, Imperial College of Science, Technology and Medicine (1993).

[6] S. Toninel, H. Forkel, T. Frank, B. Durst, C. Hasse, and D. Linse, SAE Int. J. Engines (2009).

[7] R. R. Maly and R. Herweg, SAE Paper **922243** (1992).

[8] O. L. Gulder, 23^th Symposium (International) on Combustion pages 835–842 (1990).

[9] H. G. Weller, G. Tabor, A. D. Gosman, and C. Fureby, Proceedings of the Twenty-Seventh Combustion Symposium (International) pp. 899–907 (1998).

[10] X. Yang, A. Solomon, and T. Kuo, SAE Paper **2012-01-0147** (2012).

[11] T. Lucchini, L. Cornolti, G. Montenegro, G. D'Errico, M. Fiocco, A. Teraji, and T. Shiraishi, SAE Paper **2013-01-1087** (2013).
[12] X. Zhu, L. Sforza, T. Ranadive, A. Zhang, S. Y. Lee, J. Naber, T. Lucchini, A. Onorati, M. Anbarasu, and Y. Zeng, SAE Int. J. Engines **9**, 1494–1511 (2016).
[13] L. Sforza, T. Lucchini, A. Onorati, X. Zhu, and S. Lee, "Modeling ignition and premixed combustion including flame stretch effects," in *WCX¢ 17: SAE World Congress Experience* (SAE International, 2017).
[14] R. R. Maly and R. Herveg, SAE Paper **922243** (1992).
[15] C. Chen and A. Veshagh, "A Premixed Turbulent Flame Velocity Model Based on Dimensional Reasoning," in *International Congress & Exposition* (SAE International, 1991).
[16] C. R. Choi and K. Y. Huh, Combustion and Flame. **114**, 336–348 (1998).
[17] O. L. Gulder, Proceedings the Twenty-Third Syposium on Combustion (International) pp. 743–750 (1990).
[18] O. L. Gulder, "Correlations of Laminar Combustion Data for Alternative S.I. Engine Fuels," in *SAE Technical Paper*, 841000 (1984).
[19] T. Lucchini, G. D'Errico, A. Onorati, A. Frassoldati, and A. S. annd Gilles Hardy, SAE International Journal of Engines **2**, 593–607 (2017).
[20] T. Lucchini, A. D. Torre, G. D'Errico, G. Montenegro, M. Fiocco, and A. Maghbouli, SAE Paper **2015-01-0376** (2015).
[21] C. Angelberger, T. Poinsot, and B. Delhay, "Improving near-wall combustion and wall heat transfer modeling in si engine computations," in *SAE Technical Paper* (SAE International, 1997).
[22] G. Gianetti, L. Sforza, T. Lucchini, G. D'Errico, P. Soltic, J. Rojewski, and G. Hardy, "Cfd modeling of combusiton of a natural gas light-duty engine," in *Energy Procedia*, Vol. 148 (2018), pp. 954–961.
[23] M. Reyes, F. V. Tinaut, B. Gimnez, and A. Prez, Fuel **140**, 752–761 (2015).